ACS APPLIED MATERIALS & INTERFACES

www.acsami.org

Research Article

Metal Nanoparticles/MoS_2 Surface-Enhanced Raman Scattering-Based Sandwich Immunoassay for α-Fetoprotein Detection

Engin Er, Ana Sánchez-Iglesias, Alessandro Silvestri, Blanca Arnaiz, Luis M. Liz-Marzán,* Maurizio Prato,* and Alejandro Criado*

Cite This: *ACS Appl. Mater. Interfaces* 2021, 13, 8823–8831

Read Online

ACCESS | Metrics & More | Article Recommendations | Supporting Information

ABSTRACT: The detection of cancer biomarkers at an early stage of tumor development is vital for effective diagnosis and treatment of cancer. Current diagnostic tools can often detect cancer only when the biomarker levels are already too high, so that the tumors have spread and treatments are less effective. It is urgent therefore to develop highly sensitive assays for the detection of such biomarkers at the lowest possible concentration. In this context, we developed a sandwich immunoassay based on surface-enhanced Raman scattering (SERS) for the ultrasensitive detection of α-fetoprotein (AFP), which is typically present in human serum as a biomarker indicative of early stages of hepatocellular carcinoma. In the immunoassay design, molybdenum disulfide (MoS_2) modified with a monoclonal antibody was used as a capture probe for AFP. A secondary antibody linked to an SERS-encoded nanoparticle was employed as the Raman signal reporter, that is, the transducer for AFP detection. The sandwich immunocomplex "capture probe/target/SERS tag" was deposited on a silicon wafer and decorated with silver-coated gold nanocubes to increase the density of "hot spots" on the surface of the immunosensor. The developed SERS immunosensor exhibits a wide linear detection range (1 pg mL^{-1} to 10 ng mL^{-1}) with a limit of detection as low as 0.03 pg mL^{-1} toward AFP with good reproducibility (RSD < 6%) and stability. These parameters demonstrate that the proposed immunosensor has the potential to be used as an analytical platform for the detection of early-stage cancer biomarkers in clinical applications.

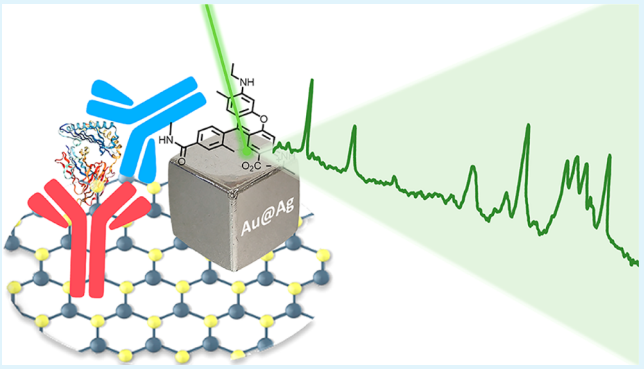

KEYWORDS: *molybdenum disulfide, Au−Ag core−shell nanostructures, immunosensor, surface-enhanced Raman scattering (SERS), α-fetoprotein*

INTRODUCTION

Early diagnosis technologies are of crucial importance in modern medicine, especially to reduce the amount of deaths caused by cancer.[1] Therefore, the ultrasensitive and selective detection of cancer biomarkers has attracted great attention as a means to diagnose and monitor tumor occurrence and progression. With currently available diagnostic methods, it is still challenging to detect cancer biomarkers at low-level concentrations in the body. In particular, such an ultrasensitive detection is essential for liver cancer, which is one of the most common and aggressive cancers worldwide and has no therapeutic options when not diagnosed at an early stage.

Alpha-fetoprotein (AFP) is a plasma protein mainly found in human fetuses. During pregnancy, elevated AFP concentrations in maternal serum may indicate spina bifida and anencephaly,[2] whereas decreased AFP levels in the second trimester of pregnancy are evaluated within risk assessment for trisomy 21 (Down syndrome) in combination with human chorionic gonadotropin beta (hCG + β) among other parameters, such as gestational age and maternal weight.[3] In addition, AFP is an important diagnostic tumor-specific biomarker for different types of cancers. AFP is normally produced in trace amounts (5−10 ng mL^{-1}) in healthy adult organs such as yolk sac and liver.[4] In 1964, AFP was first described as a human tumor-associated protein by Tatarinov.[5] Afterward, it was proven that high amounts of AFP (>400 ng mL^{-1}) in individuals are indicative of malignant diseases such as non-seminomatous testicular cancer and primary hepatocellular carcinoma (HCC).[6,7] Elevated AFP levels in human serum have occasionally been found in association with gastrointestinal tract cancers. Therefore, the early detection of AFP levels in human blood would play a crucial role in the prevention of different diseases.

Received: December 15, 2020
Accepted: January 19, 2021
Published: February 13, 2021

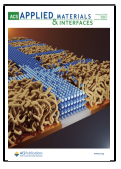

https://dx.doi.org/10.1021/acsami.0c22203
ACS Appl. Mater. Interfaces 2021, 13, 8823−8831

A wide range of diagnostic techniques have been proposed for the detection of serum AFP, such as polymerase chain reaction assay,[8] immunoradiometric assay,[9] magnetic resonance immunoassay,[10] aptamer-based fluorescent assay,[11] fluorometric immunoassays,[11−15] chemiluminescence assays,[16−20] electrochemical assays,[21−25] and metamaterial-assisted terahertz spectroscopy,[26] among others.[27−29] However, most of these approaches present limited reliability and sensitivity for AFP or they are time-consuming and require the use of complex instruments. Thus, the development of alternative diagnostic techniques for the detection of AFP as a biomarker is still required.

Surface-enhanced Raman scattering (SERS) has become one of the most promising analytical techniques[30] owing to its high sensitivity, capable of reaching the single molecule detection limit under certain conditions, and selectivity related to the specific peaks for vibrational modes, resulting in molecular fingerprints. SERS-based immunoassays have been shown to constitute a promising approach for highly sensitive AFP detection.[31,32] Such SERS-based immunoassays generally utilize a standard protocol of sandwich structure composed of three elements: (i) a primary antibody immobilized on the support surface, (ii) an analyte-specific SERS tag, which is linked to (iii) a secondary antibody.[33] Shape-controlled metal nanoparticles (NPs) such as nanospheres,[34] nanorods,[35] nanostars,[36] nanocubes,[37,38] and so forth are excellent candidates for the fabrication of SERS substrates due to their intrinsically intense plasmonic response as well as the potential formation of "hotspots". Alternatively, metal/semiconductor hybrid systems have been recently described as highly efficient SERS substrates.[39] On the other hand, molybdenum disulfide (MoS_2), one of the most interesting two-dimensional (2D) layered nanomaterials,[40] features promising properties toward biosensing applications, such as SERS performance,[41,42] high surface area, and adsorption capability for biomolecules by chemical functionalization, to originate stable interfaces.[43] Additionally, the various possibilities for chemical modification largely reduce the potential risk that might be derived from the biodegradability of MoS_2 in biological systems.[44−48] The combination of plasmonic NPs with 2D nanomaterials such as MoS_2, $MoSe_2$, and graphene has been recently reported as an interesting alternative approach for highly efficient SERS substrates.[49−53] For example, Su et al. achieved a high density of gold NPs (AuNPs) by *in situ* growth on MoS_2 nanosheets, thereby producing hot spots for SERS activity amplification.[54]

We present herein an SERS-based sandwich immunoassay comprising a monoclonal antibody (mAb) covalently attached to a MoS_2 surface as the capture substrate and a rhodamine 6G (R6G)-labeled mAb as the SERS probe. Quantitative and rapid AFP detection is achieved by decoration with plasmonic NPs. The covalent immobilization of proteins usually provides a strong and stable attachment, whereas physical adsorption affords only short-term retention of the biological activity. Chemically exfoliated MoS_2 was selected as a substrate due to its potential for large-scale production and high surface area. Monodispersed gold nanospheres (AuNSPs) and silver-coated gold nanocubes (Au@AgNCs) were used as Raman signal enhancers to increase the sensitivity of the SERS immunosensor. The proposed SERS-based sandwich immunoassay exhibits an extremely high sensitivity toward the detection of AFP (LOD as low as 0.03 pg mL^{-1}), with high stability, even in blood plasma.

EXPERIMENTAL SECTION

Chemicals and Reagents. MoS_2 (~6 μm), iodine (I_2), 1,2-dimethoxyethane, gold (III) chloride trihydrate ($HAuCl_4 \cdot 3H_2O \geq$ 99.9%), hexadecyltrimethylammonium chloride (CTAC, 25% in water), sodium borohydride ($NaBH_4$, 99%), hexadecyltrimethylammonium bromide (CTAB, ≥99.0%), benzyldimethylammonium chloride (BDAC, ≥98.0%), L-ascorbic acid (AA, ≥99%), silver nitrate ($AgNO_3$, ≥99%), phosphate buffer saline (PBS), Tween20, bovine serum albumin (BSA, 96%), *N*-(3-dimethylaminopropyl)-*N*′-ethylcarbodiimide hydrochloride (EDC, 98%), *N*-hydroxysuccinimide (NHS, 98%), and R6G (99%) were purchased from Sigma-Aldrich (Madrid, Spain). 5-Carboxy-R6G (C-R6G) was purchased from Santa Cruz Biotechnology Inc. (Dallas, USA). Human α_1-fetoprotein (ab112246) and α_1-fetoprotein monoclonal and polyclonal antibodies (ab8201 and ab54745) were purchased from Abcam PLC Inc. (Cambridge, UK). All chemicals, including organic solvents used in reactions, purification, and SERS analysis, were purchased from either Sigma-Aldrich or Alfa Aesar and used as received. Human blood serum was purchased from Sigma-Aldrich. All reagents and chemicals were of analytical grade and used without further purification. Milli-Q water (resistivity 18.2 MΩ·cm at 25 °C) was used in the preparation of plasmonic NPs. All glassware and stirrer bars were washed with aqua regia.

Apparatus and Measurements. The prepared nanomaterials were characterized by Raman spectroscopy, X-ray photoelectron spectroscopy (XPS), UV−Vis−NIR spectroscopy, and transmission electron microscopy (TEM). Raman spectra were recorded with a Renishaw Invia Raman spectrometer equipped with a green laser (λ = 532 nm) and plotted after baseline correction by means of the Wire 4.3 software. XPS measurements were performed in a SPECS Sage HR 100 spectrometer with a nonmonochromatic X-ray source of aluminum with a Kα line of 1486.6 eV energy and 300 W. Fitting of XPS data was carried out using CasaXPS software. UV−Vis−NIR spectra were recorded with an Agilent 8453 UV−Vis spectrophotometer. TEM images were obtained with a JEOL JEM-1400 PLUS transmission electron microscope operating at an acceleration voltage of 120 kV, equipped with a GATAN US1000 CCD camera. Thermogravimetric analysis (TGA) was performed with a TA Instruments Discovery system under air.

Synthesis of AuNSPs. Gold seeds (~1.5 nm) were prepared by fast reduction of $HAuCl_4$ (5 mL, 0.25 mM) with freshly prepared $NaBH_4$ (0.3 mL, 10 mM) in aqueous CTAB solution (100 mM) under vigorous stirring for 2 min at room temperature and then kept undisturbed at 27 °C for 30 min to ensure complete decomposition of sodium borohydride.[55] The mixture turned from light yellow to brownish, indicating the formation of gold seeds. An aliquot of the seed solution (0.6 mL) was added under vigorous stirring to a growth solution containing CTAC (100 mL, 100 mM), $HAuCl_4$ (0.36 mL, 50 mM), and ascorbic acid (0.36 mL, 100 mM). The mixture was left undisturbed for 12 h at 25 °C. The solution containing 10 nm AuNPs was centrifuged (9000 rpm, 2 h) to remove excess CTAC and ascorbic acid and redispersed in water to a final gold concentration equal to 2.5 mM. To grow 10 nm AuNSPs up to 58 nm diameter, a volume of gold seed solution (0.05 mL, 2.5 mM) was added under vigorous stirring to a growth solution containing BDAC (50 mL, 100 mM), $HAuCl_4$ (0.5 mL, 0.5 mM), and ascorbic acid (0.5 mL, 100 mM). The mixture was left undisturbed for 30 min at 30 °C and then washed twice by centrifugation (6000 rpm, 30 min). Finally, the NPs were redispersed in CTAB (0.5 mM) to a final gold concentration of 1.0 mM. The diameter of the obtained AuNSPs was 58 ± 1 nm.

Synthesis of Silver-Coated Gold Nanocubes (Au@AgNCs). To overgrow AuNPs with silver,[56] to a solution of 58 nm AuNSPs (10 mL, 0.25 mM) in BDAC (10 mM) at 60 °C, we added solutions of $AgNO_3$ (0.15 mL, 10 mM) and AA (0.06 mL, 100 mM) under vigorous stirring for 1 h. The solution containing silver-coated AuNPs was centrifuged (8000 rpm, 1 h) to remove excess BDAC and ascorbic acid and redispersed in CTAB (0.5 mM) to a final gold concentration of 1 mM. The side length of the obtained silver-coated gold truncated nanocubes was 62 ± 1 nm.

https://dx.doi.org/10.1021/acsami.0c22203
ACS Appl. Mater. Interfaces 2021, 13, 8823−8831

Scheme 1. Schematic Representation of the SERS Immunosensor Based on Au@AgNCs/MoS_2 Hybrid Nanomaterial

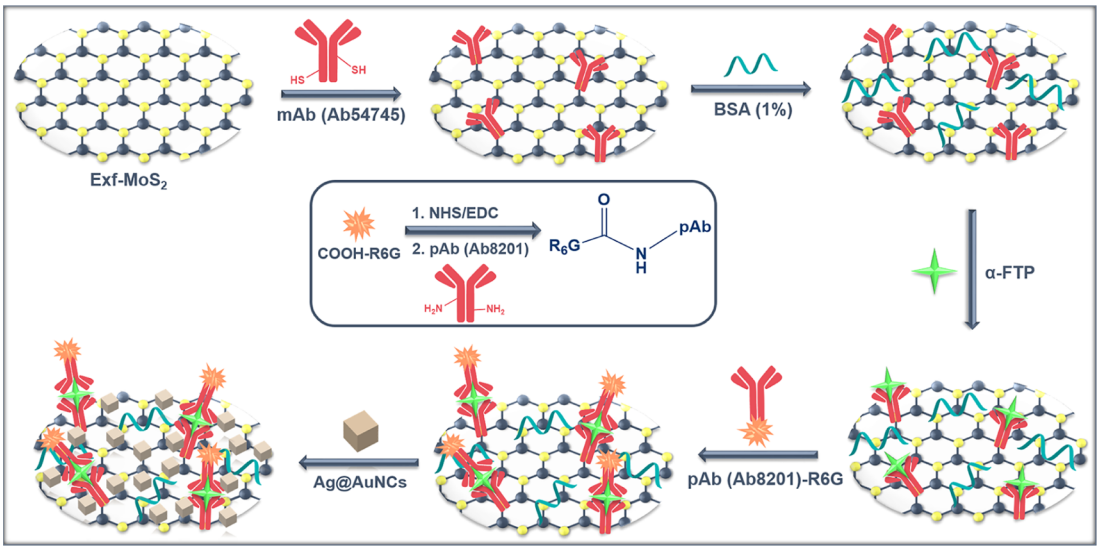

Preparation of mAb@MoS_2. Few-layer MoS_2 nanosheets were exfoliated by NaK alloys according to our previous report.[57] Subsequently, exfoliated MoS_2 (Exf-MoS_2) was sonicated in Milli-Q water using a tip sonicator in order to increase the active surface sides of the material. Exf-MoS_2 suspension was filtrated using a PTFE membrane filter (0.45 μM) and then dried under vacuum at room temperature. The apparent thickness and lateral dimension of Exf-MoS_2 were 220 ± 116 nm (Figure S1) and of 567 ± 239 nm (Figure S2), respectively. Exf-MoS_2 (3 mg) was mixed with capture mAb (Ab54745, Abcam) in PBS (pH 7.2) and then sonicated in an ice bath for 10 min.[58] The suspension was then mildly shaken inside an ice bath for 24 h. The resulting mixture was centrifuged five times with PBS (pH 7.2) at 1109 g using a centrifuge tube with a cut-off membrane (300 kDa) and then dialyzed in PBS (pH 7.2) using a dialysis tubing system (300 kDa) to remove non-attached mAb. To block mAb-bound MoS_2 (mAb@MoS_2) and to avoid degradation of MoS_2 under environmental conditions, 500 μL of BSA (1%, w/v) in PBS (pH 7.4) was added to the mAb@MoS_2 solution (1 mg mL^{-1}, 1 mL) and incubated for 1 h at 37 °C. Afterward, the mixture was extensively washed with 0.05% Tween-20 in PBS (PBST) and with fresh PBS solution. A final concentration of mAb@MoS_2 solution was adjusted to 1 mg mL^{-1} for the sandwich immunoassay system. The adsorption of mAb on Exf-MoS_2 was characterized by TGA as presented in Figure S3.

Preparation of the Ab-R6G Complex as a SERS Tag. R6G, as a Raman reporter molecule, was conjugated with a secondary antibody (Ab8201, Abcam) by means of the well-known carbodiimide cross-linker reaction.[59] For this purpose, EDC (0.384 mg, 2 μmol), NHS (0.230 mg, 2 μmol), and carboxylated-R6G (0.495 mg, 1 μmol) were added to an Ab solution (0.2 mL, 1 mg mL^{-1}) in 2.0 mL of PBS (pH 7.4) under shaking at room temperature for 3 h. The solution was then dialyzed five times with PBS solution using a cut-off dialysis bag (10 kDa) until the complete removal of unattached carboxylated-R6G. The solution was concentrated to 0.5 mL by centrifugation with cut-off membrane tubes (50 kDa) and monitored by cleaning the Ab-R6G complex with fresh PBS solution until no free residual carboxylated-R6G was detected in the solution.

Immunoassay Protocol for AFP Detection. (I) 100 μL aliquots at selected AFP concentrations were added to each of the BSA-blocked mAb@MoS_2 solutions (100 μL, 1 mg mL^{-1}) and incubated for 1 h at 37 °C. Then, the mixture was washed five times with fresh PBST solutions. (II) 100 μL aliquots of Ab@R6G solutions were added to each of the AFP-captured mAb@MoS_2 solutions and incubated for 1 h at 37 °C. Then, the mixture was extensively washed again with fresh PBST solutions and fresh PBS solutions for purification. (III) The purified immune-SERS composites containing different AFP concentrations were dispersed in 100 μL of Milli-Q water for 5 min, followed by drop-casting 5 μL of each SERS composite onto a silicon wafer (5 mm × 5 mm) and drying at room temperature. (IV) As a final step, 5 μL of Au@AgNCs was deposited by drop-casting onto each of the silicon wafers coated with the immuno-sandwich assay system and subsequently washed with water to remove unattached NPs.

RESULTS AND DISCUSSION

Immunoassay Sensing Strategy. Scheme 1 represents the design of the SERS immunoassay based on the combination of a MoS_2 substrate and Au@AgNCs. In our design, chemically exfoliated MoS_2 was first prepared by treatment with a NaK alloy and then functionalized with an AFP-selective mAb for use as a capture probe for AFP. The exfoliation process facilitated the production of MoS_2 with a highly enriched 1T phase, having improved SERS activity as compared to that of bulk MoS_2 in a 2H phase due to its enhanced charge-transfer ability.[57] It should be noted that the use of Exf-MoS_2 with a rough surface results in an effective bioconjugation with the mAb, likely through a non-specific adsorption.[60] We subsequently used dilute BSA as a blocking agent to prevent the non-specific adsorption of the analyte on the MoS_2 surface as well as to prevent the degradation of MoS_2.[44−48] On the other hand, R6G was attached by amide bonding to the secondary (detection) mAb and used as an SERS reporter. In the sensing step, R6G-labeled mAb should recognize the target AFP, previously captured by the mAb-modified MoS_2 substrate. Finally, Au@AgNCs were deposited over the surface to enhance the sensitivity of the SERS immunosensor toward AFP. The choice of Au@AgNCs was motivated by their SERS-enhancing efficiency,[61−63] so that both the localized surface plasma resonance band of Au@AgNCs and the absorption band of R6G are resonant with the 532 nm laser (Figure S4). Indeed, Hwang et al. have recently developed a similar ultrasensitive SERS system based on the AgNCs/MoS_2 platform that is able to detect R6G under 532 nm excitation.[64] With this configuration, the developed SERS immunosensor presents several advantages: (i) direct anchoring of mAb on MoS_2 with no need for linker molecules such as mercaptobenzoic acid or thiolated-PEG, (ii) avoiding the use of metal nanostructure-based SERS tags and their potential

https://dx.doi.org/10.1021/acsami.0c22203
ACS Appl. Mater. Interfaces 2021, 13, 8823−8831

degradation by oxidation of the metal (Ag in particular) during the functionalization step.[65,66]

Characterization of Au@AgNCs/MoS_2. The chemical composition, crystalline structure, optical properties, and morphology of the synthesized nanomaterials were investigated by XPS, Raman and UV−Vis spectroscopies, and TEM. The crystallinity and phase transition of MoS_2 samples were confirmed by Raman spectroscopy and XPS (Figures S5−S7). The obtained results demonstrate the successful exfoliation of MoS_2 with a high proportion of the 1T phase (~93%). As shown in Figure S4, the characteristic plasmon band of AuNSPs at 532 nm was shifted to lower wavelengths after silver overgrowth, as expected. Shown in Figure 1 are representative TEM images of monodisperse and smooth AuNSPs with a size of around 58 nm as well as cubic and slightly truncated Au@AgNCs upon Ag reduction on the AuNSP cores.

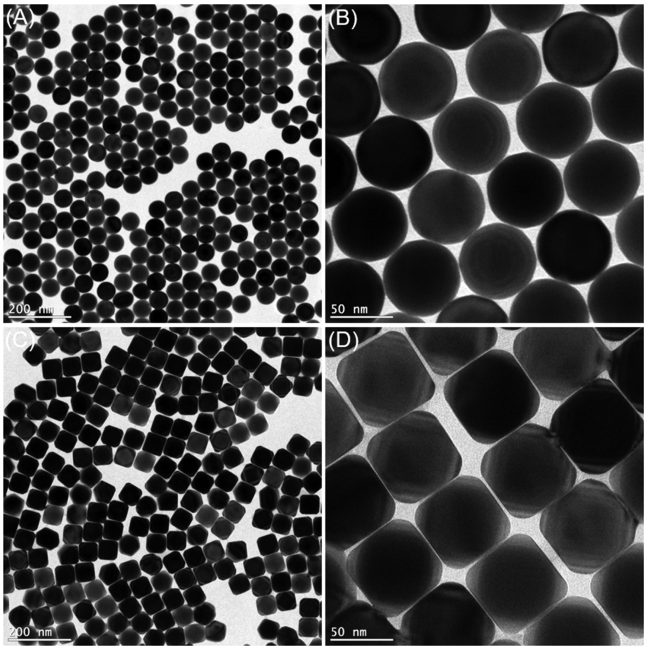

Figure 1. Representative TEM images of AuNSPs (A,B) and Au@AgNCs (C,D) at two different magnifications.

Characterization of SERS Substrates. To demonstrate the feasibility of the developed NPs/MoS_2-based substrate as a sensing platform, the SERS performance was first evaluated by directly adsorbing the Raman reporter R6G (in the absence of an immunoassay and target analyte) on MoS_2. For this purpose, SERS-active substrates were prepared on a silicon wafer, comprising a 300 nm SiO_2 layer on a Si(100) surface, by drop-casting chemically exfoliated MoS_2 (MoS_2/SiO_2) and then plasmonic NPs on the MoS_2 surface (AuNSPs/MoS_2/SiO_2 and Au@AgNCs/MoS_2/SiO_2). Subsequently, the prepared NPs/MoS_2-based SERS substrates were immersed in an R6G solution for 2 h to achieve a homogenous interaction on the whole SERS substrate with the Raman reporter and then rinsed thoroughly with Milli-Q water and dried under a nitrogen flow. The surface morphology of the prepared SERS substrates was analyzed by SEM. Figure 2 shows few-layered MoS_2 nanosheets with micron-sized diameters, on which spherical AuNSPs and cubic-shaped Au@AgNCs are deposited with uniform distribution.

All modified SERS substrates were analyzed by Raman spectroscopy, using a 532 nm excitation laser at a power of 1.6 mW/μm^2 and a collection time of 10 s. SERS spectra of R6G on MoS_2/SiO_2, AuNSPs/MoS_2/SiO_2, and Au@AgNCs/MoS_2/SiO_2 substrates are compared in Figure 3A. The characteristic SERS peaks of R6G at 1360 and 1648 cm^{-1}, which are assigned to C−H bending vibrations in aromatic rings, were clearly observed for all the substrates.[67] This result confirmed that exfoliated MoS_2 displays SERS-enhancing activity, owing to its superior charge-transfer ability, as previously reported.[57,68] The deposition of AuNPs on MoS_2/SiO_2 remarkably enhanced the SERS intensities of R6G at 1360 and 1648 cm^{-1} due to their strong plasmonic response. We can also conclude from Figure 3B that the SERS activity of Au@AgNCs on MoS_2/SiO_2 was significantly higher (~×1.5 times) than that of AuNSPs toward R6G at both selected Raman shifts due to the stronger SERS enhancement ability of AgNPs.[69] Indeed, although both samples are resonant with the 532 nm laser line, AuNSPs present high damping rates at this wavelength via interband transitions, resulting in a decay of the SERS effect.[61−63] Therefore, Au@AgNCs/MoS_2/SiO_2 was selected as an SERS platform for further immunosensing experiments.

Analytical Performance. The detection efficiency of the SERS immunosensor for quantitative AFP analysis was evaluated by recording SERS signals for different AFP concentrations. The vibrational signal at 1648 cm^{-1}, which is the most intense and characteristic peak for R6G, was selected as the analytical parameter for AFP detection. For each concentration, five replicate measurements were recorded using the developed SERS immunosensor under optimized conditions. The intensity of the SERS peak at 1648 cm^{-1} was found to gradually increase for increasing AFP concentrations, ranging from 0.001 to 10 ng mL^{-1} in PBS (pH 7.2) and human serum, as shown in Figure 4A. The corresponding calibration curves for both media in Figures 4B and S8 demonstrate a good linearity between the peak intensities at 1648 cm^{-1} and

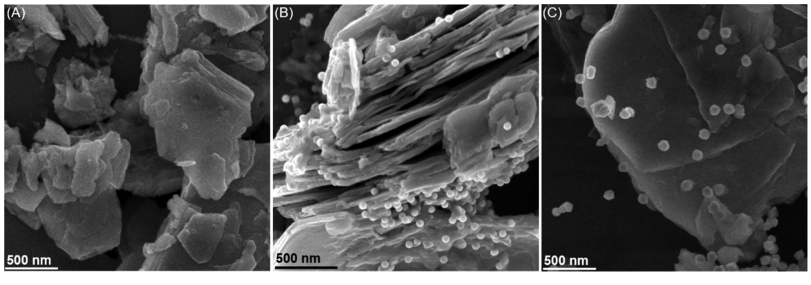

Figure 2. SEM images of (A) MoS_2 nanosheets, (B) AuNSPs/MoS_2, and (C) Au@AgNCs/MoS_2.

https://dx.doi.org/10.1021/acsami.0c22203
ACS Appl. Mater. Interfaces 2021, 13, 8823−8831

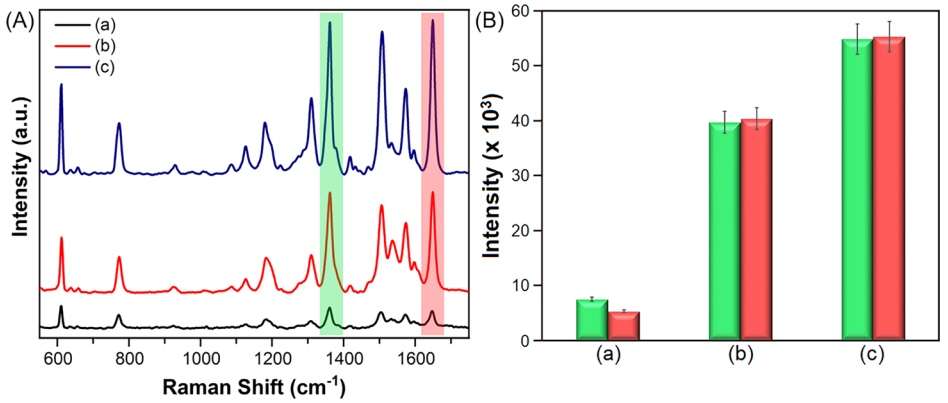

Figure 3. (A) SERS spectra for 1.0 μM R6G drop-casted on MoS_2/SiO_2 (a), AuNSPs/MoS_2/SiO_2 (b), and Au@AgNCs/MoS_2/SiO_2 (c); (B) comparison of the SERS intensities at 1360 cm^{-1} (green columns) and 1648 cm^{-1} (red columns) for 1.0 μM R6G drop-casted on MoS_2/SiO_2 (a), AuNSPs/MoS_2/SiO_2 (b), and Au@AgNCs/MoS_2/SiO_2 (c).

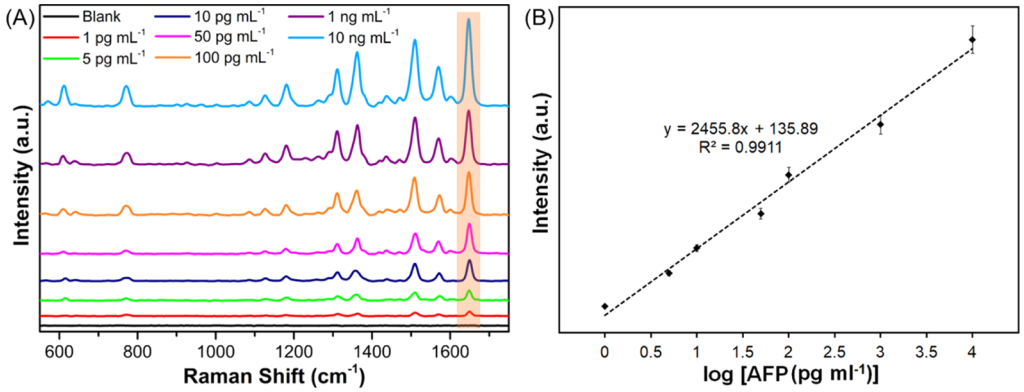

Figure 4. (A) SERS spectra of R6G at different concentrations of target AFP, ranging from 1 pg mL^{-1} to 10 ng mL^{-1} on the developed sandwich immunosensor; (B) linear plot of the Raman peak intensity at 1648 cm^{-1} as a function of the logarithm of the AFP concentration in PBS (pH 7.2) media (error bars indicate the standard deviation obtained from five different measurements).

Table 1. Comparison of Analytical Performance of Different SERS Immunosensors toward AFP Detection

material	linear range	LOD	refs
AgNF-branched DNA	(0.067–670 ng mL^{-1})[a]	(0.067 ng mL^{-1})[a]	31
Au@Ag nanospheres	0.5–100 pg mL^{-1}	0.08 pg mL^{-1}	70
SiO_2@Ag microspheres	2.1 fg mL^{-1}–21 ng mL^{-1}	2.10 fg mL^{-1}	71
gold–silica alloy core shell	0.2–22 ng mL^{-1}	0.10 ng mL^{-1}	72
SiC@Ag film	1 fg mL^{-1}–100 pg mL^{-1}	0.46 fg mL^{-1}	73
MBA-AuNPs	1–100 ng mL^{-1}	100 pg mL^{-1}	74
AuNS@Ag@SiO_2	3 pg mL^{-1}–3 μg mL^{-1}	0.72 pg mL^{-1}	75
AgNPs trimer	(0.0134–1.34 fg mL^{-1})	6.5 ag mL^{-1}	76
Au@AgNCs/MoS_2/SiO_2	1 pg mL^{-1} – 10 ng mL^{-1}	0.03 pg mL^{-1}	this work

[a]In this value, it is assumed that the target analyte is recombinant AFP with a molecular weight of 67 kDa.

the logarithm of AFP concentrations, in the same range. The linear regression equations obtained in PBS and human serum were determined as $y = 2455.5x + 201.7$ ($R^2 = 0.9911$) and $y = 2550.8x - 69.799$ ($R^2 = 0.9917$), respectively, where y is the average intensity of SERS signals at 1648 cm^{-1} and x is the logarithm of AFP concentration. The LOD value for AFP in human serum was estimated to be 0.03 pg mL^{-1} (~0.08 fM) using the following equation: LOD = $3S/m$, where S is the standard deviation of 10 replicate SERS spectra at the lowest concentration of the calibration line and m is the slope of the calibration line. In addition, the Raman spectrum of a control sample showed no discernible signal in the absence of AFP, meaning that unspecific adsorption is negligible in this system.

A comparison of the analytical performance of the developed SERS-based immunoassay with similar studies reported in the literature (Table 1) demonstrates its potential as an alternative sensing platform with high sensitivity toward AFP detection.

In order to reveal the specific role played by MoS_2 in the SERS immunosensor, we compared its analytical performance with that of a traditional ELISA surface based on polystyrene in the absence of MoS_2 but using the same sandwich immunoassay protocol. It is worth noting that both sensors involve a similar practicality and rapidity, around 3 h, which is comparable to similar SERS biosensors.[64] Figure 5 summarizes the sensitivity of the immunosensors at different AFP concentrations (1.0 to 1000.0 pg mL^{-1}). The results

https://dx.doi.org/10.1021/acsami.0c22203
ACS Appl. Mater. Interfaces 2021, 13, 8823–8831

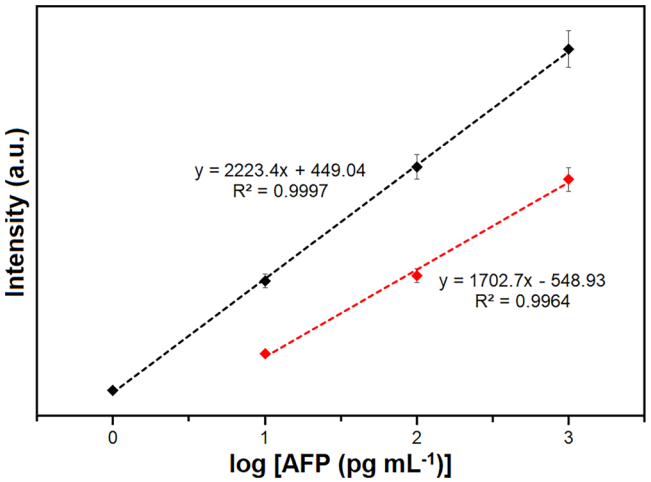

Figure 5. Comparison of the SERS intensity at 1648 cm^{-1} vs logarithmic concentration of AFP at the MoS_2-based SERS immunosensor (black line) and conventional ELISA immunosensor (red line).

consistently demonstrate a superior sensitivity of the immunosensor involving MoS_2, which we assign to the high available surface area and the excellent adsorption capability of the corresponding mAb onto MoS_2, which facilitate the interaction between the mAb-functionalized immunosensor surface and AFP molecules.

Reproducibility and Stability. The reproducibility and stability of the MoS_2-based SERS immunosensor were also investigated by analyzing AFP (1.0 ng mL^{-1}) under optimal experimental conditions. After incubation with AFP solution and with the secondary antibody, SERS spectra were randomly collected from 20 different spots on the SERS immunosensor (Figure S9). The relative standard deviation (RSD) value of the SERS spectra at 1648 cm^{-1} for AFP was found to be 5.5%. It was also observed from stability measurements (n = 3) that 94.2% of the Raman response of AFP at 1648 cm^{-1} on the first day was maintained after 2 weeks of storage (Figure S10). We thus conclude that the MoS_2-based immunosensor features high reproducibility and stability toward AFP detection.

Analysis in Serum. The potential analytical application of the developed SERS immunosensor for the detection of AFP was evaluated by using human blood serum samples. Considering the average concentration of AFP in blood serum of cancer patients, blood serum samples were spiked in the absence and in the presence of AFP and then stored at −20 °C prior to SERS analysis. SERS spectra were recorded by the immunosensor as a function of AFP concentration in blood serum, and the amount of AFP was calculated based on the R6G Raman signal at 1648 cm^{-1} (Figure S11). As summarized in Table 2, average recovery values were found between 96.9 and 104.8% with low RSD values. In addition, a control experiment with zero AFP concentration in serum was performed, showing no R6G Raman signals (Figure S12). These results suggest that our SERS-based immunosensor has not only high sensitivity but also remarkable accuracy for the detection of AFP in human serum. Furthermore, these experiments demonstrate that no interference occurs due to the presence of other plasma components, considering that the plasma contains various other proteins such as human serum albumin, globulins, and fibrinogens, with 6 orders of magnitude higher concentrations as compared to AFP.[77]

Table 2. Quantification of AFP in Human Serum Using the SERS-Based Immunosensor (n = 3)

sample	spiked concentration (pg mL^{-1})	detected concentration (pg mL^{-1})	recovery (%)	RSD (%)
human serum	0	not detected		
	10	10.38	103.8	3.71
	100	96.87	96.9	0.69
	1000	1048.2	104.8	2.78

CONCLUSIONS

A SERS-based immunosensor with an ad hoc-devised architecture has been developed for the ultrasensitive detection of the cancer biomarker AFP. This immunosensor shows remarkably high sensitivity and a reliable detection range from 1.0 pg mL^{-1} to 10.0 ng mL^{-1} with a competitive LOD of 0.03 pg mL^{-1} compared to previously reported systems. The developed immunosensor presents several advantages such as cost efficiency, fast response, high sensitivity, and reproducibility toward AFP detection. In addition, the developed MoS_2-based immunosensor was successfully applied to detect AFP in human serum samples with good recoveries, demonstrating that other species present in serum do not interfere with AFP detection. The proposed sandwich-type immunoassay could become an alternative candidate for the early diagnosis of AFP and other biomarkers in clinical applications.

ASSOCIATED CONTENT

Supporting Information

The Supporting Information is available free of charge at https://pubs.acs.org/doi/10.1021/acsami.0c22203.

TEM, SEM, TGA, Raman, and XPS analyses of Exf-MoS_2; UV spectra of plasmonic nanostructures; calibration plot; and SERS spectra of AFP for validation studies (PDF)

AUTHOR INFORMATION

Corresponding Authors

Luis M. Liz-Marzán − *Center for Cooperative Research in Biomaterials (CIC BiomaGUNE), Basque Research and Technology Alliance (BRTA), 20014 Donostia-San Sebastián, Spain; Centro de Investigación Biomédica en Red, Bioingeniería, Biomateriales y Nanomedicina (CIBER-BBN), 20014 Donostia-San Sebastián, Spain; Department of Applied Chemistry, University of the Basque Country, 20018 Donostia-San Sebastián, Spain; Ikerbasque, Basque Foundation for Science, 48013 Bilbao, Spain;* orcid.org/0000-0002-6647-1353; Email: llizmarzan@cicbiomagune.es

Maurizio Prato − *Center for Cooperative Research in Biomaterials (CIC BiomaGUNE), Basque Research and Technology Alliance (BRTA), 20014 Donostia-San Sebastián, Spain; Ikerbasque, Basque Foundation for Science, 48013 Bilbao, Spain; Department of Chemical and Pharmaceutical Sciences, Universitá Degli Studi di Trieste, 34127 Trieste, Italy;* orcid.org/0000-0002-8869-8612; Email: prato@units.it

Alejandro Criado − *Center for Cooperative Research in Biomaterials (CIC BiomaGUNE), Basque Research and Technology Alliance (BRTA), 20014 Donostia-San*

https://dx.doi.org/10.1021/acsami.0c22203
ACS Appl. Mater. Interfaces 2021, 13, 8823−8831

Sebastián, Spain; orcid.org/0000-0002-9732-513X; Email: acriado@cicbiomagune.es

Authors

Engin Er − *Center for Cooperative Research in Biomaterials (CIC BiomaGUNE), Basque Research and Technology Alliance (BRTA), 20014 Donostia-San Sebastián, Spain; Department of Analytical Chemistry, Faculty of Pharmacy, Ankara University, 06560 Ankara, Turkey*

Ana Sánchez-Iglesias − *Center for Cooperative Research in Biomaterials (CIC BiomaGUNE), Basque Research and Technology Alliance (BRTA), 20014 Donostia-San Sebastián, Spain; Centro de Investigación Biomédica en Red, Bioingeniería, Biomateriales y Nanomedicina (CIBER-BBN), 20014 Donostia-San Sebastián, Spain;* orcid.org/0000-0003-1871-8742

Alessandro Silvestri − *Center for Cooperative Research in Biomaterials (CIC BiomaGUNE), Basque Research and Technology Alliance (BRTA), 20014 Donostia-San Sebastián, Spain*

Blanca Arnaiz − *Center for Cooperative Research in Biomaterials (CIC BiomaGUNE), Basque Research and Technology Alliance (BRTA), 20014 Donostia-San Sebastián, Spain;* orcid.org/0000-0001-5789-0321

Complete contact information is available at: https://pubs.acs.org/10.1021/acsami.0c22203

Notes

The authors declare no competing financial interest.

■ ACKNOWLEDGMENTS

E.E. is grateful for a fellowship from the Scientific and Technological Research Council of Turkey (TUBITAK). A.C. and A.S. thank MINECO for their research grant (Juan de la Cierva—Incorporación/no. IJCI-2016-31113, Juan de la Cierva—Formacion/no. FJC2018-036777-I, respectively). We thank Dr. Judith Langer for support in the interpretation of SERS results. This work was supported by the European Union's Horizon 2020 research and innovation program under Grant Agreements 785219 and 881603 Graphene Flagship. L.M.L.-M. acknowledges funding from the European Research Council (ERC-AdG-2017# 787510). M.P., as the recipient of the AXA Bionanotechnology Chair, is grateful to the AXA Research Fund for financial support. This work was performed under the Maria de Maeztu Units of Excellence Program from the Spanish State Research Agency—grant no. MDM-2017-0720.

■ REFERENCES

(1) Bray, F.; Ferlay, J.; Soerjomataram, I.; Siegel, R. L.; Torre, L. A.; Jemal, A. Global Cancer Statistics 2018: GLOBOCAN Estimates of Incidence and Mortality Worldwide for 36 Cancers in 185 Countries. *Ca-Cancer J. Clin.* **2018**, *68*, 394−424.

(2) Brock, D. J. H. Alphafetoprotein and Neural Tube Defects. *J. Clin. Pathol.* **1976**, *10*, 157−164.

(3) Wald, N. J.; Kennard, A.; Densem, J. W.; Cuckle, H. S.; Chard, T.; Butler, L. Antenatal Maternal Serum Screening for Down's Syndrome: Results of a Demonstration Project. *Br. Med. J.* **1992**, *305*, 391−394.

(4) Lee, C.-W.; Tsai, H.-I.; Lee, W.-C.; Huang, S.-W.; Lin, C.-Y.; Hsieh, Y.-C.; Kuo, T.; Chen, C.-W.; Yu, M.-C. Normal Alpha-Fetoprotein Hepatocellular Carcinoma: Are They Really Normal? *J. Clin. Med.* **2019**, *8*, 1736.

(5) Tatarinov, L. S. Detection of embryo-specific alpha-globulin in the blood serum of a patient with primary liver cancer. *Vopr. Med. Khim.* **1964**, *10*, 90−91.

(6) Bai, D. S.; Zhang, C.; Chen, P.; Jin, S. J.; Jiang, G. Q. The Prognostic Correlation of AFP Level at Diagnosis with Pathological Grade, Progression, and Survival of Patients with Hepatocellular Carcinoma. *Sci. Rep.* **2017**, *7*, 12870.

(7) Masuzaki, R.; Karp, S. J.; Omata, M. New Serum Markers of Hepatocellular Carcinoma. *Semin. Oncol.* **2012**, *39*, 434−439.

(8) Zhang, Y.; Li, T.; Qiu, Y.; Zhang, T.; Guo, P.; Ma, X.; Wei, Q.; Han, L. Serum MicroRNA Panel for Early Diagnosis of the Onset of Hepatocellular Carcinoma. *Medicine* **2017**, *96*, No. e5642.

(9) Kemp, H. A.; Simpson, J. S.; Woodhead, J. S. Automated Two-Site Immunoradiometric Assay of Human Alpha-Fetoprotein in Maternal Serum. *Clin. Chem.* **1981**, *27*, 1388−1391.

(10) Khramtsov, P.; Kropaneva, M.; Bochkova, M.; Timganova, V.; Zamorina, S.; Rayev, M. Solid-Phase Nuclear Magnetic Resonance Immunoassay for the Prostate-Specific Antigen by Using Protein-Coated Magnetic Nanoparticles. *Microchim. Acta* **2019**, *186*, 768.

(11) Xu, J.; Chen, W.; Shi, M.; Huang, Y.; Fang, L.; Zhao, S.; Yao, L.; Liang, H. An Aptamer-Based Four-Color Fluorometic Method for Simultaneous Determination and Imaging of Alpha-Fetoprotein, Vascular Endothelial Growth Factor-165, Carcinoembryonic Antigen and Human Epidermal Growth Factor Receptor 2 in Living Cells. *Microchim. Acta* **2019**, *186*, 204.

(12) Zhu, D.; Hu, Y.; Zhang, X. J.; Yang, X. T.; Tang, Y. Y. Colorimetric and Fluorometric Dual-Channel Detection of α-Fetoprotein Based on the Use of ZnS-CdTe Hierarchical Porous Nanospheres. *Microchim. Acta* **2019**, *186*, 124.

(13) Long, Y.; Zhang, Z.; Yan, X.; Xing, J.; Zhang, K.; Huang, J.; Zheng, J.; Li, W. Multiplex Immunodetection of Tumor Markers with a Suspension Array Built upon Core-Shell Structured Functional Fluorescence-Encoded Microspheres. *Anal. Chim. Acta* **2010**, *665*, 63−68.

(14) Liu, X.; Song, X.; Dong, Z.; Meng, X.; Chen, Y.; Yang, L. Photonic Crystal Fiber-Based Immunosensor for High-Performance Detection of Alpha Fetoprotein. *Biosens. Bioelectron.* **2017**, *91*, 431−435.

(15) Xie, Q.; Weng, X.; Lu, L.; Lin, Z.; Xu, X.; Fu, C. A Sensitive Fluorescent Sensor for Quantification of Alpha-Fetoprotein Based on Immunosorbent Assay and Click Chemistry. *Biosens. Bioelectron.* **2016**, *77*, 46−50.

(16) Fu, Z.; Yan, F.; Liu, H.; Yang, Z.; Ju, H. Channel-Resolved Multianalyte Immunosensing System for Flow-through Chemiluminescent Detection of α-Fetoprotein and Carcinoembryonic Antigen. *Biosens. Bioelectron.* **2008**, *23*, 1063−1069.

(17) Yang, X.-Y.; Guo, Y.-S.; Bi, S.; Zhang, S.-S. Ultrasensitive Enhanced Chemiluminescence Enzyme Immunoassay for the Determination of α-Fetoprotein Amplified by Double-Codified Gold Nanoparticles Labels. *Biosens. Bioelectron.* **2009**, *24*, 2707−2711.

(18) Hu, Q.; Yang, J.; Zheng, Z.; Ding, Y.; Chen, Y.; Gao, W. In Situ H_2O_2 Generation with Gold Nanoflowers as the Coreactant Accelerator for Enzyme-Free Electrochemiluminescent Immunosensing. *Biosens. Bioelectron.* **2019**, *143*, 111627.

(19) Chen, Y.; Sun, J.; Xianyu, Y.; Yin, B.; Niu, Y.; Wang, S.; Cao, F.; Zhang, X.; Wang, Y.; Jiang, X. A Dual-Readout Chemiluminescent-Gold Lateral Flow Test for Multiplex and Ultrasensitive Detection of Disease Biomarkers in Real Samples. *Nanoscale* **2016**, *8*, 15205−15212.

(20) Huang, X.; Ren, J. Gold Nanoparticles Based Chemiluminescent Resonance Energy Transfer for Immunoassay of Alpha Fetoprotein Cancer Marker. *Anal. Chim. Acta* **2011**, *686*, 115−120.

(21) Zhang, S.; Cao, W.; Li, J.; Su, M. MCE Enzyme Immunoassay for Carcinoembryonic Antigen and Alpha-Fetoprotein Using Electrochemical Detection. *Electrophoresis* **2009**, *30*, 3427−3435.

(22) Niu, Y.; Yang, T.; Ma, S.; Peng, F.; Yi, M.; Wan, M.; Mao, C.; Shen, J. Label-Free Immunosensor Based on Hyperbranched Polyester for Specific Detection of α-Fetoprotein. *Biosens. Bioelectron.* **2017**, *92*, 1−7.

(23) Gan, N.; Jin, H.; Li, T.; Zheng, L. Fe_3O_4/Au Magnetic Nanoparticle Amplification Strategies for Ultrasensitive Electrochemical Immunoassay of Alfa-Fetoprotein. *Int. J. Nanomed.* **2011**, *6*, 3259−3269.
(24) Liang, W.; Yi, W.; Li, S.; Yuan, R.; Chen, A.; Chen, S.; Xiang, G.; Hu, C. A Novel, Label-Free Immunosensor for the Detection of α-Fetoprotein Using Functionalised Gold Nanoparticles. *Clin. Biochem.* **2009**, *42*, 1524−1530.
(25) Ding, Y.; Liu, J.; Wang, H.; Shen, G.; Yu, R. A Piezoelectric Immunosensor for the Detection of α-Fetoprotein Using an Interface of Gold/Hydroxyapatite Hybrid Nanomaterial. *Biomaterials* **2007**, *28*, 2147−2154.
(26) Geng, Z.; Zhang, X.; Fan, Z.; Lv, X.; Chen, H. A Route to Terahertz Metamaterial Biosensor Integrated with Microfluidics for Liver Cancer Biomarker Testing in Early Stage. *Sci. Rep.* **2017**, *7*, 16378.
(27) Lu, L.; Yu, J.; Liu, X.; Yang, X.; Zhou, Z.; Jin, Q.; Xiao, R.; Wang, C. Rapid, Quantitative and Ultra-Sensitive Detection of Cancer Biomarker by a SERRS-Based Lateral Flow Immunoassay Using Bovine Serum Albumin Coated Au Nanorods. *RSC Adv.* **2019**, *10*, 271−281.
(28) Zhu, Y.; Zhang, Q.; Li, X.; Pan, H.; Wang, J.; Zhao, Z. Detection of AFP with an Ultra-Sensitive Giant Magnetoimpedance Biosensor. *Sens. Actuators, B* **2019**, *293*, 53−58.
(29) Wang, Q.; Hu, Y.; Jiang, N.; Wang, J.; Yu, M.; Zhuang, X. Preparation of Aptamer Responsive DNA Functionalized Hydrogels for the Sensitive Detection of α-Fetoprotein Using SERS Method. *Bioconjugate Chem.* **2020**, *31*, 813−820.
(30) Langer, J.; Jimenez de Aberasturi, D.; Alvarez-Puebla, R. A.; Auguié, B.; Baumberg, J. J.; Bazan, G. C.; Bell, S. E. J.; Boisen, A.; Brolo, A. G.; Choo, J.; Cialla-May, D.; Deckert, V.; Fabris, L.; Faulds, K.; García de Abajo, F. J.; Goodacre, R.; Graham, D.; Haes, A. J.; Haynes, C. L.; Huck, C.; Itoh, T.; Käll, M.; Kneipp, J.; Kotov, N. A.; Kuang, H.; Le Ru, E. C.; Lee, H. K.; Li, J.-F.; Ling, X. Y.; Maier, S. A.; Mayerhöfer, T.; Moskovits, M.; Murakoshi, K.; Nam, J.-M.; Nie, S.; Ozaki, Y.; Pastoriza-Santos, I.; Perez-Juste, J.; Popp, J.; Pucci, A.; Reich, S.; Ren, B.; Schatz, G. C.; Shegai, T.; Schlücker, S.; Tay, L.-L.; Thomas, K. G.; Tian, Z.-Q.; Van Duyne, R. P.; Vo-Dinh, T.; Wang, Y.; Willets, K. A.; Xu, C.; Xu, H.; Xu, Y.; Yamamoto, Y. S.; Zhao, B.; Liz-Marzán, L. M. Present and Future of Surface-Enhanced Raman Scattering. *ACS Nano* **2020**, *14*, 28−117.
(31) Cheng, L.; Zhang, Z.; Zuo, D.; Zhu, W.; Zhang, J.; Zeng, Q.; Yang, D.; Li, M.; Zhao, Y. Ultrasensitive Detection of Serum MicroRNA Using Branched DNA-Based SERS Platform Combining Simultaneous Detection of α-Fetoprotein for Early Diagnosis of Liver Cancer. *ACS Appl. Mater. Interfaces* **2018**, *10*, 34869−34877.
(32) Chen, R.; Liu, B.; Ni, H.; Chang, N.; Luan, C.; Ge, Q.; Dong, J.; Zhao, X. Vertical Flow Assays Based on Core-Shell SERS Nanotags for Multiplex Prostate Cancer Biomarker Detection. *Analyst* **2019**, *144*, 4051−4059.
(33) Song, C.; Chen, J.; Zhao, Y.; Wang, L. Gold-Modified Silver Nanorod Arrays for SERS-Based Immunoassays with Improved Sensitivity. *J. Mater. Chem. B* **2014**, *2*, 7488−7494.
(34) Ashley, M. J.; Bourgeois, M. R.; Murthy, R. R.; Laramy, C. R.; Ross, M. B.; Naik, R. R.; Schatz, G. C.; Mirkin, C. A. Shape and Size Control of Substrate-Grown Gold Nanoparticles for Surface-Enhanced Raman Spectroscopy Detection of Chemical Analytes. *J. Phys. Chem. C* **2018**, *122*, 2307−2314.
(35) Lin, K.-Q.; Yi, J.; Hu, S.; Liu, B.-J.; Liu, J.-Y.; Wang, X.; Ren, B. Size Effect on SERS of Gold Nanorods Demonstrated via Single Nanoparticle Spectroscopy. *J. Phys. Chem. C* **2016**, *120*, 20806−20813.
(36) Villa, J. E. L.; Garcia, I.; Jimenez de Aberasturi, D.; Pavlov, V.; Sotomayor, M. D. P. T.; Liz-Marzán, L. M. SERS-Based Immunoassay for Monitoring Cortisol-Related Disorders. *Biosens. Bioelectron.* **2020**, *165*, 112418.
(37) Liu, Y.; Zhou, J.; Wang, B.; Jiang, T.; Ho, H.-P.; Petti, L.; Mormile, P. Au@Ag Core-Shell Nanocubes: Epitaxial Growth Synthesis and Surface-Enhanced Raman Scattering Performance. *Phys. Chem. Chem. Phys.* **2015**, *17*, 6819−6826.
(38) Omar, R.; En Naciri, A.; Jradi, S.; Battie, Y.; Toufaily, J.; Mortada, H.; Akil, S. One-Step Synthesis of a Monolayer of Monodisperse Gold Nanocubes for SERS Substrates. *J. Mater. Chem. C* **2017**, *5*, 10813−10821.
(39) Zhou, L.; Zhou, J.; Lai, W.; Yang, X.; Meng, J.; Su, L.; Gu, C.; Jiang, T.; Pun, E. Y. B.; Shao, L.; Petti, L.; Sun, X. W.; Jia, Z.; Li, Q.; Han, J.; Mormile, P. Irreversible Accumulated SERS Behavior of the Molecule-Linked Silver and Silver-Doped Titanium Dioxide Hybrid System. *Nat. Commun.* **2020**, *11*, 1785.
(40) Huang, X.; Zeng, Z.; Zhang, H. Metal Dichalcogenide Nanosheets: Preparation, Properties and Applications. *Chem. Soc. Rev.* **2013**, *42*, 1934−1946.
(41) Yan, D.; Qiu, W.; Chen, X.; Liu, L.; Lai, Y.; Meng, Z.; Song, J.; Liu, Y.; Liu, X.-Y.; Zhan, D. Achieving High-Performance Surface-Enhanced Raman Scattering through One-Step Thermal Treatment of Bulk MoS_2. *J. Phys. Chem. C* **2018**, *122*, 14467−14473.
(42) Lee, Y.; Kim, H.; Lee, J.; Yu, S. H.; Hwang, E.; Lee, C.; Ahn, J.-H.; Cho, J. H. Enhanced Raman Scattering of Rhodamine 6G Films on Two-Dimensional Transition Metal Dichalcogenides Correlated to Photoinduced Charge Transfer. *Chem. Mater.* **2016**, *28*, 180−187.
(43) Hirsch, A.; Hauke, F. Post-Graphene 2D Chemistry: The Emerging Field of Molybdenum Disulfide and Black Phosphorus Functionalization. *Angew. Chem., Int. Ed.* **2018**, *57*, 4338−4354.
(44) Wang, Z.; Von Dem Bussche, A.; Qiu, Y.; Valentin, T. M.; Gion, K.; Kane, A. B.; Hurt, R. H. Chemical Dissolution Pathways of MoS_2 Nanosheets in Biological and Environmental Media. *Environ. Sci. Technol.* **2016**, *50*, 7208−7217.
(45) Nurdiwijayanto, L.; Ma, R.; Sakai, N.; Sasaki, T. Stability and Nature of Chemically Exfoliated MoS2 in Aqueous Suspensions. *Inorg. Chem.* **2017**, *56*, 7620−7623.
(46) Lee, T.-W.; Chen, C.-C.; Chen, C. Chemical Stability and Transformation of Molybdenum Disulfide Nanosheets in Environmental Media. *Environ. Sci. Technol.* **2019**, *53*, 6282−6291.
(47) Kurapati, R.; Muzi, L.; de Garibay, A. P. R.; Russier, J.; Voiry, D.; Vacchi, I. A.; Chhowalla, M.; Bianco, A. Enzymatic Biodegradability of Pristine and Functionalized Transition Metal Dichalcogenide MoS_2 Nanosheets. *Adv. Funct. Mater.* **2017**, *27*, 1605176.
(48) Martín, C.; Kostarelos, K.; Prato, M.; Bianco, A. Biocompatibility and Biodegradability of 2D Materials: Graphene and Beyond. *Chem. Commun.* **2019**, *55*, 5540−5546.
(49) Zhang, Y.; Chen, W.; Fu, T.; Sun, J.; Zhang, D.; Li, Y.; Zhang, S.; Xu, H. Simultaneous Surface-Enhanced Resonant Raman and Fluorescence Spectroscopy of Monolayer $MoSe_2$: Determination of Ultrafast Decay Rates in Nanometer Dimension. *Nano Lett.* **2019**, *19*, 6284−6291.
(50) Zhang, D.; Wu, Y. C.; Yang, M.; Liu, X.; Coileain, C. O.; Abid, M.; Abid, M.; Wang, J. J.; Shvets, I.; Xu, H.; Chun, B. S.; Liu, H.; Wu, H. C. Surface Enhanced Raman Scattering of Monolayer MX_2 with Metallic Nano Particles. *Sci. Rep.* **2016**, *6*, 30320.
(51) Wang, Z.; Wu, S.; Colombi Ciacchi, L.; Wei, G. Graphene-Based Nanoplatforms for Surface-Enhanced Raman Scattering Sensing. *Analyst* **2018**, *143*, 5074−5089.
(52) Shorie, M.; Kumar, V.; Kaur, H.; Singh, K.; Tomer, V. K.; Sabherwal, P. Plasmonic DNA Hotspots Made from Tungsten Disulfide Nanosheets and Gold Nanoparticles for Ultrasensitive Aptamer-Based SERS Detection of Myoglobin. *Microchim. Acta* **2018**, *185*, 158.
(53) Pramanik, A.; Gao, Y.; Gates, K.; Begum, S.; Ray, P. C. Giant Chemical and Excellent Synergistic Raman Enhancement from a 3D $MoS_{2-x}O_x$−Gold Nanoparticle Hybrid. *ACS Omega* **2019**, *4*, 11112−11118.
(54) Su, S.; Zhang, C.; Yuwen, L.; Chao, J.; Zuo, X.; Liu, X.; Song, C.; Fan, C.; Wang, L. Creating SERS Hot Spots on MoS_2 Nanosheets with in Situ Grown Gold Nanoparticles. *ACS Appl. Mater. Interfaces* **2014**, *6*, 18735−18741.
(55) Zheng, Y.; Zhong, X.; Li, Z.; Xia, Y. Successive, Seed-Mediated Growth for the Synthesis of Single-Crystal Gold Nanospheres with

https://dx.doi.org/10.1021/acsami.0c22203
ACS Appl. Mater. Interfaces 2021, 13, 8823−8831

Uniform Diameters Controlled in the Range of 5-150 Nm. *Part. Part. Syst. Charact.* **2014**, *31*, 266−273.
(56) Gómez-Graña, S. Au@Ag Nanoparticles: Halides Stabilize {100} Facets. *J. Phys. Chem. Lett.* **2013**, *4*, 2209−2216.
(57) Er, E.; Hou, H.-L.; Criado, A.; Langer, J.; Möller, M.; Erk, N.; Liz-Marzán, L. M.; Prato, M. High-Yield Preparation of Exfoliated 1T-MoS_2 with SERS Activity. *Chem. Mater.* **2019**, *31*, 5725−5734.
(58) Juzgado, A.; Soldà, A.; Ostric, A.; Criado, A.; Valenti, G.; Rapino, S.; Conti, G.; Fracasso, G.; Paolucci, F.; Prato, M. Highly Sensitive Electrochemiluminescence Detection of a Prostate Cancer Biomarker. *J. Mater. Chem. B* **2017**, *5*, 6681−6687.
(59) Song, C.; Min, L.; Zhou, N.; Yang, Y.; Su, S.; Huang, W.; Wang, L. Synthesis of Novel Gold Mesoflowers as SERS Tags for Immunoassay with Improved Sensitivity. *ACS Appl. Mater. Interfaces* **2014**, *6*, 21842−21850.
(60) Tuteja, S. K.; Duffield, T.; Neethirajan, S. Liquid Exfoliation of 2D MoS_2 Nanosheets and Their Utilization as a Label-Free Electrochemical Immunoassay for Subclinical Ketosis. *Nanoscale* **2017**, *9*, 10886−10896.
(61) Yang, Y.; Shi, J.; Kawamura, G.; Nogami, M. Preparation of Au-Ag, Ag-Au Core-Shell Bimetallic Nanoparticles for Surface-Enhanced Raman Scattering. *Scr. Mater.* **2008**, *58*, 862−865.
(62) Fernanda Cardinal, M.; Rodríguez-González, B.; Alvarez-Puebla, R. A.; Pérez-Juste, J.; Liz-Marzán, L. M. Modulation of Localized Surface Plasmons and SERS Response in Gold Dumbbells through Silver Coating. *J. Phys. Chem. C* **2010**, *114*, 10417−10423.
(63) Ding, S.-J.; Zhu, J. Tuning the Surface Enhanced Raman Scattering Activity of Gold Nanocubes by Silver Coating. *Appl. Surf. Sci.* **2015**, *357*, 487−492.
(64) Tegegne, W. A.; Su, W.-N.; Tsai, M.; Bedemo, A.; Hwang, B. Ag Nanocubes Decorated 1T-MoS_2 Nanosheets SERS Substrate for Reliable and Ultrasensitive Detection of Pesticides. *Appl. Mater. Today* **2020**, *21*, 100871.
(65) Kim, C.; Galloway, J. F.; Lee, K. H.; Searson, P. C. Universal Antibody Conjugation to Nanoparticles Using the Fcγ Receptor i (FcγRI): Quantitative Profiling of Membrane Biomarkers. *Bioconjugate Chem.* **2014**, *25*, 1893−1901.
(66) Byzova, N. A.; Safenkova, I. V.; Slutskaya, E. S.; Zherdev, A. V.; Dzantiev, B. B. Less Is More: A Comparison of Antibody-Gold Nanoparticle Conjugates of Different Ratios. *Bioconjugate Chem.* **2017**, *28*, 2737−2746.
(67) Jensen, L.; Schatz, G. C. Resonance Raman Scattering of Rhodamine 6G as Calculated Using Time-Dependent Density Functional Theory. *J. Phys. Chem. A* **2006**, *110*, 5973−5977.
(68) Yin, Y.; Miao, P.; Zhang, Y.; Han, J.; Zhang, X.; Gong, Y.; Gu, L.; Xu, C.; Yao, T.; Xu, P.; Wang, Y.; Song, B.; Jin, S. Significantly Increased Raman Enhancement on MoX_2 (X=S,Se) Monolayers upon Phase Transition. *Adv. Funct. Mater.* **2017**, *27*, 1606694.
(69) Erol, M.; Han, Y.; Stanley, S. K.; Stafford, C. M.; Du, H.; Sukhishvili, S. SERS Not to Be Taken for Granted in the Presence of Oxygen. *J. Am. Chem. Soc.* **2009**, *131*, 7480−7481.
(70) Yang, L.; Gao, M. X.; Zhan, L.; Gong, M.; Zhen, S. J.; Huang, C. Z. An Enzyme-Induced Au@Ag Core-Shell NanoStructure Used for an Ultrasensitive Surface-Enhanced Raman Scattering Immunoassay of Cancer Biomarkers. *Nanoscale* **2017**, *9*, 2640−2645.
(71) Wang, X.; Zhou, L.; Wei, G.; Jiang, T.; Zhou, J. SERS-Based Immunoassay Using a Core-Shell SiO_2@Ag Immune Probe and Ag-Decorated NiCo2O4 Nanorods Immune Substrate. *RSC Adv.* **2016**, *6*, 708−715.
(72) Wang, S.; Qin, Y.; Zou, Z. Determination of Liver Cancer Biomarkers by Surface-Enhanced Raman Scattering Using Gold-Silica Nanoparticles. *Anal. Lett.* **2016**, *49*, 1209−1220.
(73) Zhou, L.; Zhou, J.; Feng, Z.; Wang, F.; Xie, S.; Bu, S. Immunoassay for Tumor Markers in Human Serum Based on Si Nanoparticles and SiC@Ag SERS-Active Substrate. *Analyst* **2016**, *141*, 2534−2541.
(74) Wang, A.; Ruan, W.; Song, W.; Chen, L.; Zhao, B.; Jung, Y. M.; Wang, X. Detection of the Potential Tumor Marker of AFP Using Surface-Enhanced Raman Scattering-Based Immunoassay. *J. Raman Spectrosc.* **2013**, *44*, 1649−1653.
(75) Zhao, J.; Wu, C.; Zhai, L.; Shi, X.; Li, X.; Weng, G.; Zhu, J.; Li, J.; Zhao, J.-W. A SERS-Based Immunoassay for the Detection of α-Fetoprotein Using AuNS@Ag@SiO_2 Core-Shell Nanostars. *J. Mater. Chem. C* **2019**, *7*, 8432−8441.
(76) Wu, X.; Fu, P.; Ma, W.; Xu, L.; Kuang, H.; Xu, C. SERS-Active Silver Nanoparticle Trimers for Sub-Attomolar Detection of Alpha Fetoprotein. *RSC Adv.* **2015**, *5*, 73395−73398.
(77) Krebs, H. A. Chemical Composition of Blood Plasma and Serum. *Annu. Rev. Biochem.* **1950**, *19*, 409−430.

https://dx.doi.org/10.1021/acsami.0c22203
ACS Appl. Mater. Interfaces 2021, 13, 8823−8831